

Electrodynamics of the high-latitude trough: Its relationship with convection flows and field-aligned currents

Shasha Zou,¹ Mark B. Moldwin,¹ Michael J. Nicolls,² Aaron J. Ridley,¹ Anthea J. Coster,³ Endawoke Yizengaw,⁴ Larry R. Lyons,⁵ and Eric F. Donovan⁶

Received 5 July 2012; revised 9 January 2013; accepted 9 January 2013; published 17 May 2013.

[1] We present a detailed case study of the electrodynamics of a high-latitude trough observed at ~12 UT (~1 MLT) on 8 March 2008 using multiple instruments, including incoherent scattering radar (ISR), GPS total electron content (TEC), magnetometers, and auroral imager. The electron density within the trough dropped as much as 80% within 6 minutes. This trough was collocated with a counterclockwise convection flow vortex, indicating divergent horizontal electric fields and currents. Together with a collocated dark area shown in auroral images, the observations provide strong evidence for an existence of downward field-aligned currents (FACs) collocated with the high-latitude trough. This is further supported by assimilative mapping of ionospheric electrodynamics results. In addition, the downward FACs formed at about the same time as a substorm onset and east of the Harang reversal, suggesting it is part of the substorm current wedge. It has long been a puzzle why this type of high-latitude trough predominantly occurs just east of the Harang reversal in the postmidnight sector. We suggest that the high-latitude trough is associated with the formation of downward FACs of the substorm current system, which usually occur just east of the Harang reversal. In addition, we find that the ionospheric electron temperature within the high latitude trough decreases in the F region while increasing in the E region. We discuss possible mechanisms responsible for the complex change in electron temperature, such as ion composition change and/or presence of downward FACs.

Citation: Zou, S., M. B. Moldwin, M. J. Nicolls, A. J. Ridley, A. J. Coster, E. Yizengaw, L. R. Lyons, and E. F. Donovan (2013), Electrodynamics of the high-latitude trough: Its relationship with convection flows and field-aligned currents, *J. Geophys. Res. Space Physics*, 118, 2565–2572, doi:10.1002/jgra.50120.

1. Introduction

[2] The ionospheric troughs are regions of remarkable electron density depression at subauroral and auroral latitudes, and significant electron density gradients exist at the boundaries. The high-latitude trough is defined as the low-density region present within the auroral oval or the polar cap [Rodger *et al.*, 1992], while the mid-latitude trough is the low-density region just equatorward of the auroral oval.

Their definitions are mainly based on their relative location to the auroral oval and not their absolute latitudinal locations. Compared with the midlatitude trough, the high-latitude trough has been much less intensely studied and is thus not sufficiently understood. A review of the high-latitude trough from early studies can be found in the studies by Rodger *et al.* [1992] and Jones *et al.* [1990]. The high-latitude trough is usually accompanied by enhanced eastward convection flows, significantly enhanced ion temperature, but almost no change or even a decrease in the electron temperature and a large upward field-aligned ion velocity [Williams and Jain, 1986; Winsor *et al.*, 1986; Ma *et al.*, 2000]. Ma *et al.* [2000] also reported plasma flow shears associated with the high-latitude trough. Previous low-earth orbit (LEO) satellite observations have shown that the high-latitude trough is usually associated with depletions of atomic species (O^+ , H^+) and enhancements of molecular species (NO^+) [Grebowsky *et al.*, 1983]. The large convection flow speed and the resulting rapid recombination rate, as well as upward field-aligned ion flow velocity, have been suggested to be possible mechanisms responsible for the formation of the high-latitude trough [Winsor *et al.*, 1986; Jones *et al.*, 1990].

[3] Of particular interest is one type of high-latitude trough that is frequently found immediately east of the Harang reversal region [Jones *et al.*, 1990]. The Harang

¹Department of Atmospheric, Oceanic, and Space Sciences, University of Michigan, Ann Arbor, Michigan, USA.

²Center for Geospace Studies, SRI International, Menlo Park, California, USA.

³Haystack Observatory, Massachusetts Institute of Technology, Westford, Massachusetts, USA.

⁴Institute for Scientific Research, Boston College, Chestnut Hill, Massachusetts, USA.

⁵Department of Atmospheric and Oceanic Sciences, UCLA, Los Angeles, California, USA.

⁶Department of Physics and Astronomy, University of Calgary, Calgary, Alberta, Canada.

Corresponding author: S. Zou, Department of Atmospheric, Oceanic, and Space Sciences, University of Michigan, Ann Arbor, MI, 48109-2143, USA. (shashaz@umich.edu)

reversal [Harang, 1946; Heppner, 1972] represents a critical region in both the ionosphere and magnetosphere convection and is intrinsically associated with the Region 2 current system [Erickson *et al.*, 1991; Zou *et al.*, 2009a, 2009b, 2012; Gkioulidou *et al.*, 2009, 2011]. Recently, Zou *et al.* [2009a, 2009b] showed that the evolution of the Harang reversal is closely related to substorm development, and the substorm current wedge [McPherron *et al.*, 1973] is partially closed by the Region 2 field-aligned currents (FACs) through ionospheric Pedersen currents. In particular, Zou *et al.* [2009b] found that, east of the Harang reversal center, the electron density suddenly decreases after substorm onset and suggested that this density decrease is ultimately associated with formation of the downward FACs of the substorm current wedge. These downward FACs are at least partially closed by the Region 2 upward FACs further equatorward via enhanced equatorward Pedersen currents. This coupling is responsible for the large equatorward electric field and eastward convection flows between the downward and upward FACs pair. In this scenario, the magnetospheric process responsible for the generation of the substorm current wedge first acts as a current generator and the ionospheric electric field then modifies itself to satisfy the current continuity in the ionosphere.

[4] The purpose of this paper is to study the relationship between the high-latitude trough and the substorm/Region 2 FACs through a detailed multi-instrument case study. More specifically, we investigate whether the density decrease region formed after substorm onset exhibits similar characteristics as the high-latitude trough described in the previous literature. If so, this provides an explanation for high-latitude trough formation and for its prevalent location immediately east of the Harang reversal.

[5] Comparing the mid-latitude and the high-latitude troughs, one of the distinct differences is the different behavior of the electron temperature in these regions. It has been reported that the mean electron temperature is elevated in the mid-latitude trough region [Prölss, 2007], while the high-latitude trough case in Figure 1 in the study by Ma *et al.* [2000] clearly showed a dramatic temperature decrease. These different temperature profiles suggest that different mechanisms are responsible for the formation of these density troughs. We discuss the temperature profiles observed within the high-latitude trough region and the possible generation mechanism.

2. Observations

[6] A substorm onset occurred over Alaska at about ~1140 UT on 8 March 2008. Figure 1 shows the magnetic H component perturbations and Pi2 pulsations from three magnetometers near central Alaska. These observations have been frequently used to determine the substorm onset time. In Figure 1, the substorm onset time, indicated by magenta lines, was determined by the initiation of negative perturbation in the magnetic H component and the increase in the amplitude of the Pi2 pulsations.

[7] Figure 2 shows Poker Flat incoherent scatter radar (PFISR) observations of nightside convection flow direction (a), magnitude (b), vectors (c), and electron density at four different altitudes (d–g) from 0800 to 1230 UT. The radar run ended just before 1215 UT. The magnetic local midnight

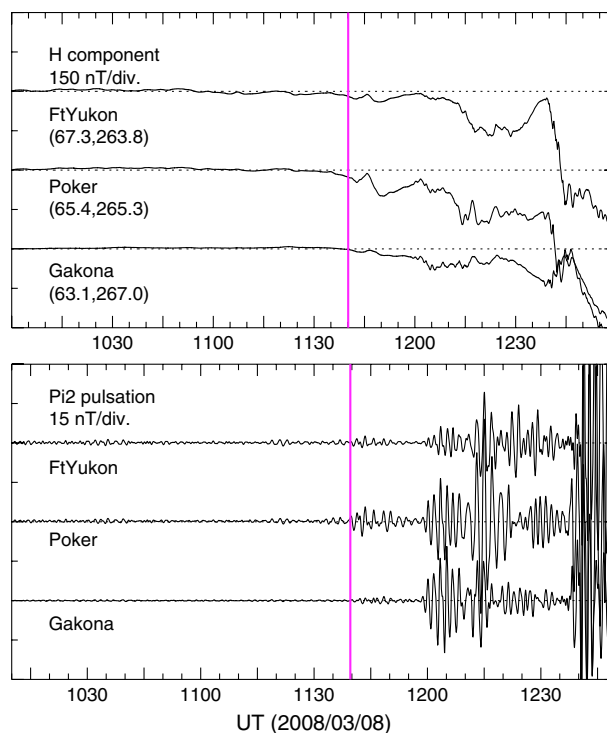


Figure 1. (a) H component perturbation measured by three magnetometers near central Alaska. (b) The Pi2 (40–150 s) filtered H component magnetometer data. The magenta lines indicate the substorm onset time.

of Poker Flat is at about 1105 UT, denoted by a triangle in Figure 2. PFISR is a part of the advanced modular incoherent scatter radar (AMISR) facility with electronic pulse-to-pulse steering capability, allowing nearly simultaneous measurement of plasma parameters in multiple look directions without physical movement of the radar antenna [Heinselman and Nicolls, 2008]. The radar run for this period used a 13-beam mode, particularly useful for monitoring the formation and evolution of ionospheric mesoscale structures. The radar beam configuration can be found in Figure 3. The radar beams are projected onto geomagnetic horizontal (Figure 3a) and meridional planes (Figure 3b). Different beams are color coded and numbered for clarification. More information about the radar transmission schemes and the methodology of the standard AMISR convection vector calculations can be found in the study by Heinselman and Nicolls [2008].

[8] As shown in Figures 2a and 2c, convection flows changed from mainly westward to eastward during this period. The transition region, i.e., the Harang reversal, was detected between 1110 and 1130 UT and is highlighted by a magenta segment in Figure 2a. Following the Harang reversal, there was a region with temporarily westward flows at higher latitude and eastward flows at lower latitudes at ~12 UT. This flow pattern suggests the existence of a counterclockwise convection flow vortex centered at ~66.25° magnetic latitude (mlat). The magnitude of the eastward flows equatorward of the center exceeded ~1500 m/s just before 12 UT. In Figures 2d–2g, electron densities measured by beams 1–4 and interpolated at four selected altitudes in the E and F regions are shown as a function of mlat of that altitude. The low-electron density region first measured at

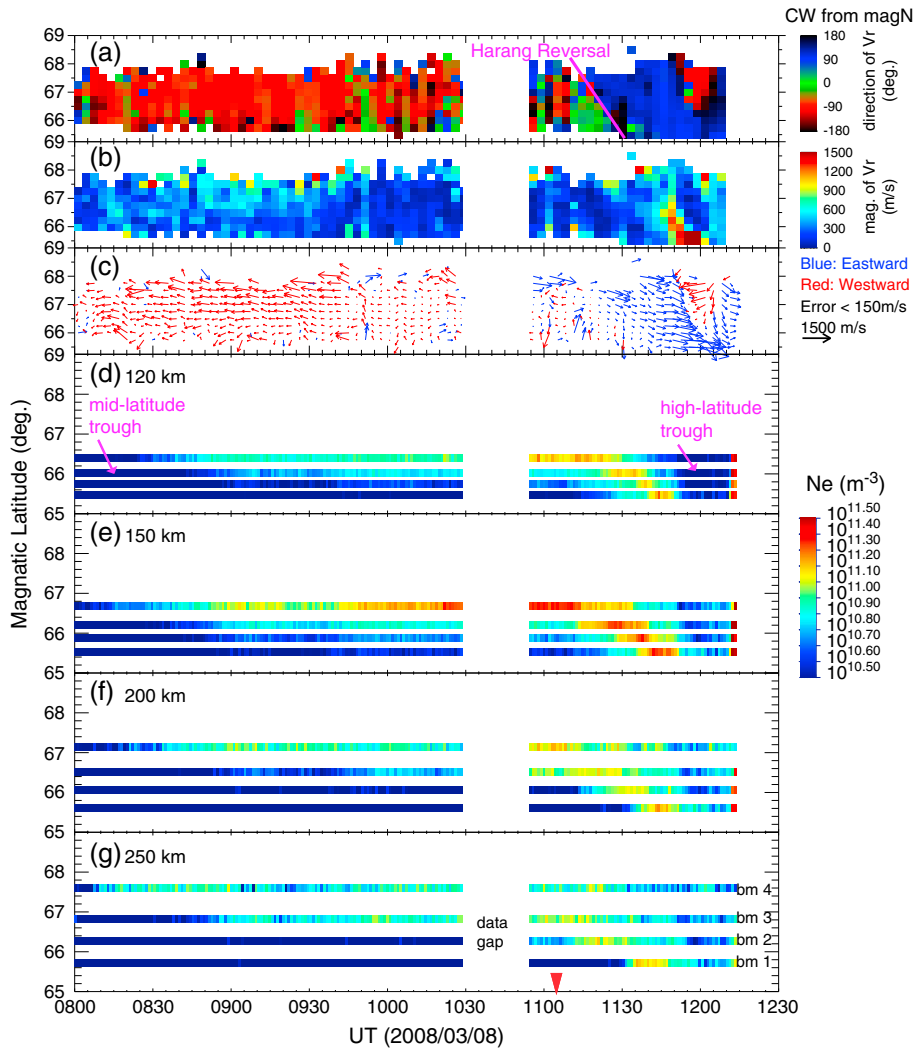


Figure 2. (a–c) Nightside convection flow direction, magnitude, and vector measured by PFISR from 0800 to 1230 UT on 8 March 2008 are shown as a function of magnetic latitude and universal time; data are plotted only if the measurement uncertainty is less than 150 m/s. In Figure 2a, the direction of the flow is zero if pointing to the magnetic north and increases (decreases) clockwise (counterclockwise). In Figure 2c, flows with eastward/westward component are blue/red. (d–g) Electron densities at four different altitudes in the E and F regions from beams 1–4. The magnetic local midnight of Poker Flat is at about 1105 UT, denoted by a triangle.

~08 UT was the poleward portion of the midlatitude trough in the subauroral region. This location for the poleward portion of the trough can also be seen in the GPS TEC observations shown in Figure 1 in the study by Zou *et al.* [2011] and through electron density observations from the CHAMP satellite from 0935 UT to 0941 UT of this day about 1 MLT west of PFISR (not shown). The dynamics of the midlatitude trough during substorms has been described in the study by Zou *et al.* [2011]. In Figure 2, electron density then increased poleward of the midlatitude trough as a result of plasma sheet particle precipitation within the auroral oval. The density depletion measured around 12 UT is the high-latitude trough, which was apparently associated with the convection vortex.

[9] The counterclockwise convection vortex suggests a divergence of the horizontal electric fields and Pedersen currents away from the vortex center. Lou [2000] studied the

divergence of the horizontal Pedersen and Hall currents as closure of FACs during substorms and found that divergence of the Pedersen currents contribute a significant portion of these FACs. Therefore, the divergence of the Pedersen currents in this case may well suggest the existence of downward FACs. The large eastward convection flows equatorward of the vortex center further suggest Pedersen currents flowing into an auroral arc equatorward of the PFISR observations (seen in the auroral images discussed later) to feed the upward FACs there. Kosch *et al.* [1998] reported a very similar plasma convection vortex eastward of the Harang reversal and poleward of an auroral arc in the postmidnight sector. Using data from magnetometers and coherent scatter radars, Kosch *et al.* [2000] were able to compute the ionospheric conductance distribution assuming a fixed Hall/Pedersen conductance ratio and then the FAC distribution using the method of characteristics [Inhyster *et al.* 1992;

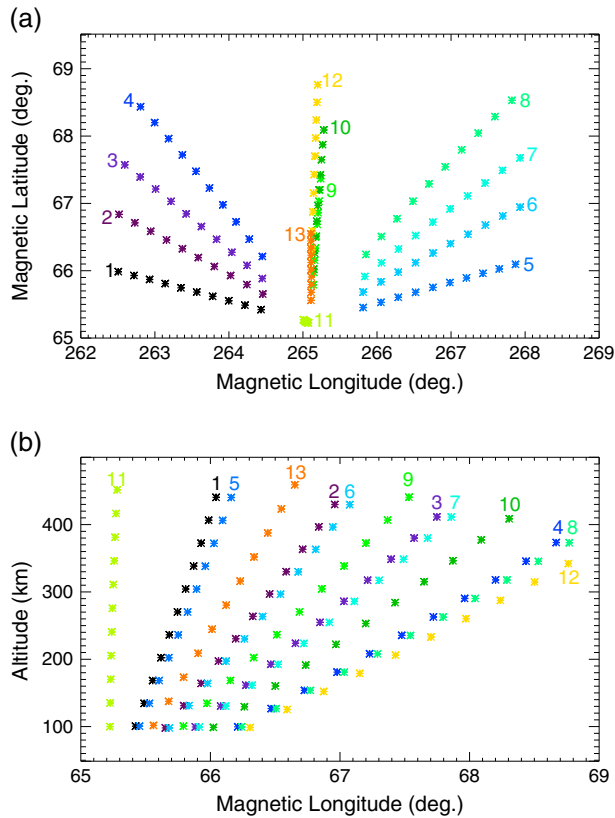


Figure 3. PFISR 13-beam radar configuration is shown in geomagnetic horizontal (a) and meridional planes (b). Different beams are color coded and numbered. Each plus sign represents the location of the data echo from the long pulse measurement.

Amm, 1995, 1998]. Their model results showed the existence of downward FACs everywhere poleward of the auroral arc. In addition, they found a low conductance region with its minimum located with the center of the counterclockwise plasma vortex. This low conductance region is now further confirmed with the direct electron density measurements from PFISR. *Kosch et al.* [2000] also mentioned that using a Hall/Pedersen conductance ratio of 1.1 and 2 within the plasma vortex region/trough do not make significant differences in the final results. These numbers are within the typical range of the Hall/Pedersen conductance ratio, while the ratio can be larger under discrete aurora.

[10] PFISR is within the field of view of the THEMIS all-sky imager (ASI) at Gakona, which is part of the THEMIS ground-based ASI array [*Mende et al.*, 2008]. The THEMIS ASI array observes the white light aurora with 1 km resolution near the center of each imager and 3 s cadence and provides information of the timing and location of auroral activities during substorms [*Donovan et al.*, 2006]. Figure 4 shows four selected auroral images taken by this ASI before the substorm onset (a); at onset, i.e., 1140 UT (b); and during the expansion phase of the substorm (c–d). The radar beams (plus signs) and ground magnetometers (red diamonds) are denoted on the auroral image. Thin dotted grey lines indicate geographic coordinates, while thicker dashed lines indicate geomagnetic coordinates. In Figures 4b and 4c, the auroral luminosity decreased near the radar site,

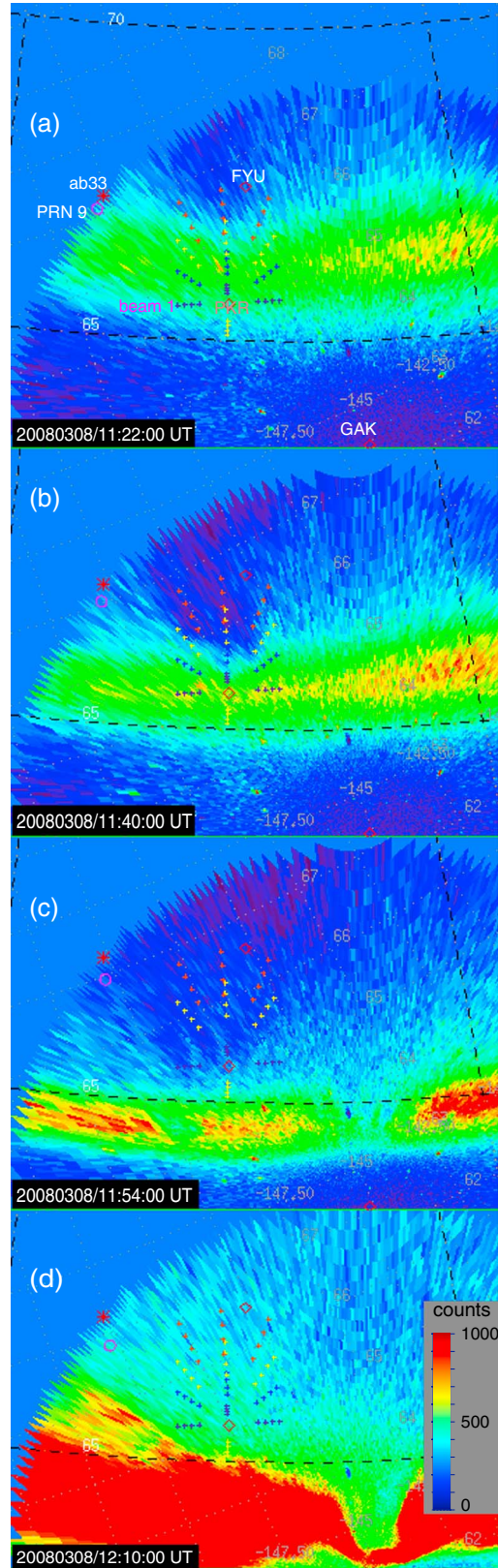


Figure 4. Aurora observations from the THEMIS ASI at Gakona. PFISR beams (plus signs) and ground magnetometers (red diamonds) used in Figure 1 are denoted. The GPS ground receiver ab33 is also shown together with the 100 km pierce point of the ray between the receiver and the GPS satellite PRN 9.

and this dark region moved gradually equatorward. The timing of the appearance and expansion of the dark region is consistent with the PFISR observation of the flow vortex and the high-latitude trough. In Figure 4d, the auroral luminosity increased because of the passage of the auroral bulge and the associated ionization is reflected by the strong electron density enhancement at the end of the radar run in Figures 2d–2g.

[11] Electric potential and FACs inferred from ground magnetometer measurements using the assimilative mapping of ionospheric electrodynamics (AMIE) technique [Richmond and Kamide, 1988; Ridley and Kihn, 2004] are shown in Figure 5. Diamonds denote the magnetometer locations. The magnetometer data are obtained from the SuperMAG website [Gjerloev, 2009]. Two magnetometers (FYU and PKR) are highlighted to show where the central Alaska meridian was at this time. This region has dense ground magnetometer distribution, so the inversion is relatively well constrained. The derived convection flow vectors at the locations of magnetometers are also shown in Figure 5, which can help to understand the PFISR observations relative to the large-scale convection flows. It can be seen that downward (upward) FACs formed near the Fort Yukon (Poker Flat) stations at higher (lower) latitudes in the postmidnight sector. The convection flows are westward poleward of the center of downward FACs and eastward equatorward of it. These results are consistent with the inferences from the PFISR measurements.

[12] Figure 6 shows the time series of vertical total electron content (VTEC) observed by GPS ground receiver ab33 from the GPS satellite PRN 9 signal. The value of the VTEC at the first data point is subtracted, so the relative change of VTEC is shown. Ab33 receiver is the closest receiver to the high-latitude trough that has data for this specific period. Both satellite and receiver interfrequency biases have been removed. The four vertical lines indicate the time when the auroral images in Figure 4 were taken. The receiver (red asterisk) and the position of ray’s 100 km pierce point (magenta circle) between the receiver and PRN 9 are also marked in Figure 4. The assumption of the raypath’s pierce point in the E region is often used for

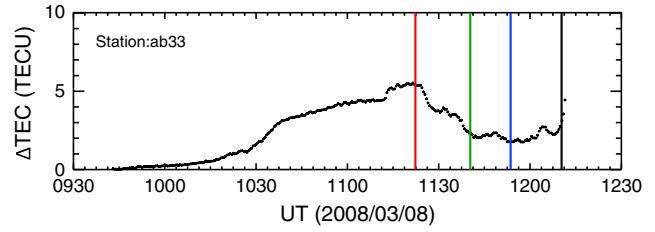


Figure 6. Time series of GPS VTEC observed by the receiver ab33. Four vertical lines correspond to the times when the aurora images were taken in Figure 4.

receivers located under active aurora [Garner *et al.*, 2011; Prikryl *et al.*, 2010]. Different altitudes of the pierce point have been tried and they were found to not affect the relative change of the TEC value, although the absolute value of the TEC would change. During this period, the pierce point of the PRN 9 satellite did not move much because it was near its highest elevation angle. The VTEC decreased ~ 4 TECU near the high-latitude trough region, and the decrease was probably even larger in the center of the trough. TEC increases and decreases have been observed at and near auroral arcs [e.g., Kintner *et al.*, 2002; Gómez *et al.*, 2007; Jayachandran *et al.*, 2009] with most emphasis being on the TEC increase. The TEC increase has been attributed to enhanced ionization associated with particle precipitating within the arc. A case study of the characteristics of TEC increase associated with an individual auroral arc is shown in the study by Kintner *et al.* [2002]. Here we suggest that the TEC decrease near but outside the auroral arc is related to downward FACs.

[13] Figure 7 shows time series of electron density (N_e), line-of-sight flow velocity (V_{los}), electron and ion temperatures (T_e and T_i) measured at four altitudes by beam 1. The geomagnetic locations and altitude where the data are recorded are listed at the top. Positive/negative V_{los} in the second panel indicates flows are away/toward the radar. The four vertical dashed lines in Figure 7 correspond to the time when the auroral images in Figure 4 were taken. The electron density decreased $\sim 80\%$ from 1.5×10^{11} to $3 \times 10^{10} \text{ #m}^{-3}$

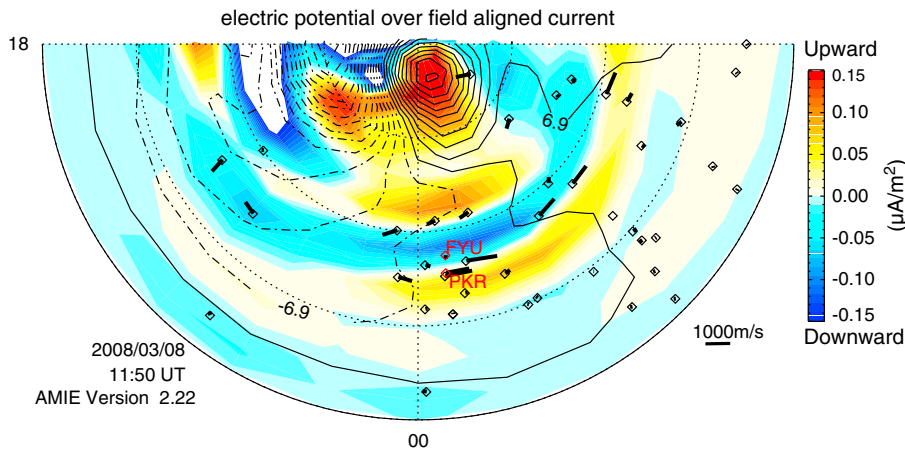


Figure 5. Electric potential and field-aligned currents calculated using the AMIE technique at 1150 UT. FYU and PKR denote the magnetometers at Fort Yukon and Poker Flat. Convection flows are also shown at the location of the magnetometers.

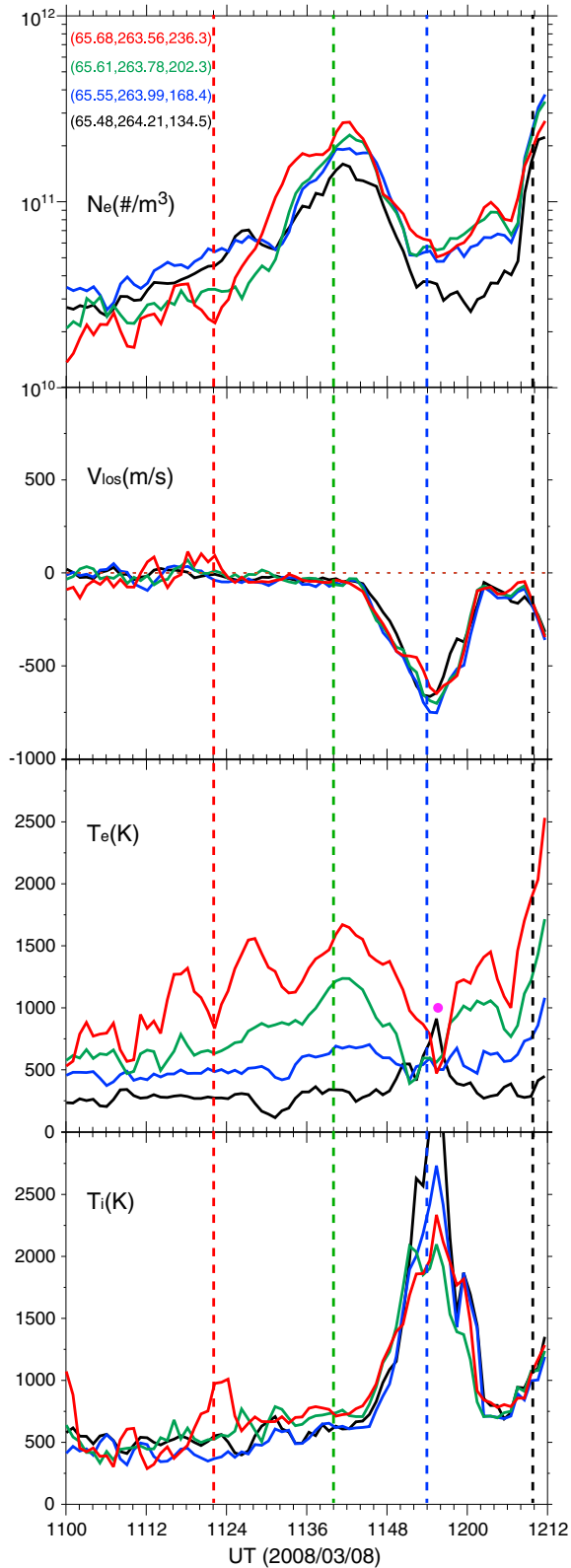


Figure 7. Time series of electron density (N_e), line-of-sight velocity (V_{los}), electron temperature (T_e), and ion temperature (T_i) measured by beam 1 at four different locations (represented by four different colors). The geomagnetic locations (lat, lon) and altitude (in km) of these locations are listed at the top. Four vertical lines correspond to the times when the aurora images were taken in Figure 4.

within ~ 6 minutes. The density decrease in the trough was also associated with a large flow speed. In the bottom panel, T_i increased significantly at all altitudes. The V_{los} and T_i observations suggest the existence of significant frictional heating between ions and neutrals. Unlike T_i , the T_e changes within the trough are much more complicated. That is T_e decreased (~ 1000 K) in the F region (red/yellow curves) but increased (~ 500 K) in the E region (black curve). The temperature dips and peaks occurred simultaneously with the V_{los} peak and the N_e minimum.

[14] As shown in Figure 7, the ion temperature is significantly elevated, and this will largely increase the charge exchange rates between O^+ and molecular species. As a result, the molecular to atomic ion transition altitude, where the ions are composed of 50% O^+ and 50% molecular ions, will rise to higher altitude. In the standard PFISR data process, ion composition is estimated using an iterative procedure assuming chemical equilibrium for the molecular species, based on the ion density calculator of *Richards et al.* [2010]. However, the calculation in *Zettergren et al.* [2010] shows that under an electric field of ~ 75 mV/m, or flow speed of about 1500 m/s, the transition altitude can rise to ~ 275 km as compared to ~ 200 km. Therefore, we have reanalyzed the PFISR data at the time of the maximum V_{los} using a fixed molecular to O^+ transition altitude of 275 km. The magenta dot indicates the refitted temperature at 236.3 km (red curve) at the peak of the flow. As can be seen, the sharp, short dip of electron temperature at ~ 236.3 km disappeared in the refitted data, which indicates that this dip could be an artificial effect of underestimated ion transition altitude. However, a smaller amplitude and broader T_e decrease can still be seen. This broader T_e decreases can also be seen at other beams at higher latitude, where the effect of the ion transition altitude is not expected to have such a significant effect because of smaller velocities.

3. Discussion

[15] Observations from PFISR and the dark area in the auroral images suggest the existence of downward FACs collocated with the high-latitude trough, and this is further confirmed with results from AMIE. Downward FACs are usually carried mainly by upward going ionospheric electrons [e.g., *Marklund, 2009*]. This indicates the possibility that reduced/no production mechanism and evacuation by downward FACs are responsible for the formation of this high-latitude trough. Calculations in the studies by *Karlsson and Marklund* [1998] and *Karlsson et al.* [2007] showed that the downward FACs are very effective in evacuating the ionosphere.

[16] Other potential processes are the rapid recombination rate following the chemical reactions converting the O^+ to molecular ions and upward flows in regions of large electric fields, which have been used to explain the formation of the high-latitude trough before [*Rodger et al., 1992* and references therein], *Sellek et al.* [1991] modeled the effect of a large (peak at 2 km/s) westward flow on the ionospheric plasma parameters. They found that the ion-neutral frictional heating significantly increase T_i and then T_e through ion-electron heat transfer. The elevated O^+ temperature and the field-aligned flows lead to a decrease in plasma density. There is also evidence of large eastward convection flows

near the equatorward portion of the high-latitude trough in this case. However, this mechanism alone is expected to lead to an enhanced electron temperature in both E and F regions, which is not consistent with observations in the F region in Figure 7.

[17] The effects of downward FACs on ionospheric T_e have been investigated both by observations and simulations. Observationally, Abe *et al.* [1991] reported T_e decreases (~ 500 – 1500 K) in the downward FAC region between 300 and 1800 km based on the Akebono satellite observations. Schunk *et al.* [1987] investigated the downward FAC effect on the electron temperature using a time-dependent 3D model. They found that FACs with magnitudes larger than $10 \mu\text{Am}^{-2}$ can have an appreciable effect on T_e , particularly during solar minimum and in winter during solar maximum. Their simulation results show that T_e decreases in the presence of downward FACs due to upward thermoelectric heat flow usually above 280 km. More recently, Zhang *et al.* [2003] used a 1D high-latitude ionospheric model to study the effect of FACs on electron temperatures. The study considered not only the thermoelectric effect but also frictional heating and expansion/contraction effects due to FACs. In their Figure 5, the altitude profile of T_e for a downward FAC with magnitude of $60 \mu\text{Am}^{-2}$ shows great similarity to our present observations. That is, T_e decreases in the F region and increases in the E region below 150 km. The E-region T_e increase has been attributed to enhanced frictional heating between electrons and neutrals. In their simulation, the dominant mechanism responsible for the F-region T_e decrease is altitude dependent. For an $8 \mu\text{Am}^{-2}$ downward FAC, the thermal electric effect is the most important energy loss term below ~ 280 km, followed by the heat advection term, while electron gas expansion is the most important mechanism for energy loss above ~ 280 km. The dependence of this critical altitude on the magnitude of FACs is not clear. Therefore, the exact mechanism responsible for the F-region T_e decrease is not known conclusively, although related with downward FACs. In addition, the magnitude of the downward FACs calculated using AMIE in the present case seems quite small compared with the currents used in these simulations. The AMIE grid cells (2° mlat and 1 MLT) are significantly larger than auroral features, so the magnitude of the FACs may be an average over stronger and weaker FACs. In addition, the estimation of the FACs magnitude may be improved by incorporating a more realistic, higher resolution conductance distribution, such as from aurora observations, in the future.

[18] In this case, the substorm onset occurred at ~ 1140 UT. The fact that this downward FAC formed at about the onset time suggests that it is the one associated with the substorm current wedge [McPherron *et al.*, 1973]. Downward FACs of the substorm current wedge are usually found to be located east of the Harang reversal [Zou *et al.*, 2009b]. Therefore, this provides an explanation of why this type of high-latitude trough preferentially occurs east of the Harang reversal, as reported by Jones *et al.* [1990].

4. Conclusions

[19] In this paper, we have presented a detailed case study of the electrodynamics of a high-latitude trough using

multiple instruments. This trough was collocated with a counterclockwise convection flow vortex with maximum eastward flow speed exceeding 1500 m/s. These observations suggest divergent electric fields and Pedersen currents and thus downward FACs. The AMIE results further confirmed the existence of the downward FACs within the high-latitude trough. The electron temperature within the trough increased in the E region but decreased in the F region. Taking into consideration the raising ion transition altitude, the magnitude of the electron temperature decrease was reduced but still significant. We discussed possible mechanisms responsible for this temperature change as well as the inference on the density drop within the trough. There is evidence of competing mechanisms operating at the same time that are responsible for the electron temperature profiles. Sophisticated ionospheric models should be used to further quantitatively study the dynamics near the high-latitude trough in the future to better understand the dependencies between the ion/electron densities and temperatures.

[20] **Acknowledgments.** The research at the University of Michigan was supported by NSF AGS1111476 and AGS1203232, NASA NNN09ZDA001N-LWSTRT and NNX114060Z-HTP. The research at the UCLA was supported by NSF AGS1042255. We thank the Geophysical Institute of the University of Alaska for the use of the 1 second GIMA ground magnetometer data. For the ground magnetometer data used in AMIE, we gratefully acknowledge the following: Intermagnet; USGS, Jeffrey J. Love; Danish Meteorological Institute; CARISMA, PI Ian Mann; CANMOS; the S-RAMP Database, PI K. Yumoto and Dr. K. Shiokawa; the SPIDR database; AARI, PI Oleg Troshichev; the MACCS program, PI M. Engbreton, Geomagnetism Unit of the Geological Survey of Canada; GIMA; MEASURE, UCLA IGPP and Florida Institute of Technology; SAMBA, PI Eftyhia Zesta; 210 Chain, PI K. Yumoto; SAMNET, PI Farideh Honary; the institutes who maintain the IMAGE magnetometer array, PI Eija Tanskanen; PENGUIN; AUTUMN, PI Martin Connors; Greenland magnetometers operated by DTU Space; South Pole and McMurdo Magnetometer, PI's Louis J. Lanzarotti and Alan T. Weatherwax; ICESAR; RAPIDMAG; PENGUIN; British Antarctic Survey; McMac, PI Dr. Peter Chi; BGS, PI Dr. Susan Macmillan; Pushkov Institute of Terrestrial Magnetism, Ionosphere and Radio Wave Propagation (IZMIRAN); SuperMAG, PI Jesper W. Gjerloev.

References

- Abe, T., T. Okuzawa, K. Oyama, H. Fukunishi, and R. Fujii (1991), Variations of thermal electron energy distribution associated with field-aligned currents, *Geophys. Res. Lett.*, *18*(2), 349–352, doi:10.1029/91GL00033.
- Amm, O. (1995), Direct determination of the local ionospheric Hall conductance distribution from two-dimensional electric and magnetic field data: Application of the method using models of typical ionospheric electrodynamic situations, *J. Geophys. Res.*, *100*, 21,473.
- Amm, O. (1998), Method of characteristics in spherical geometry applied to a Harang Discontinuity situation, *Ann. Geophys.*, *16*, 413.
- Donovan, E., et al. (2006), The azimuthal evolution of the substorm expansive phase onset aurora, in Proceedings of ICS-8, edited by M. Syrja'suo and E. Donovan, pp. 55–60, Univ. of Calgary, Calgary, Alberta, Canada.
- Erickson, G. M., R. W. Spiro, and R. A. Wolf (1991), The physics of the Harang discontinuity, *J. Geophys. Res.*, *96*, 1633–1645, doi:10.1029/90JA02344.
- Garner, T. W., R. B. Harris, J. A. York, C. S. Herbster, C. F. Minter III, and D. L. Hampton (2011), An auroral scintillation observation using precise, collocated GPS receivers, *Radio Sci.*, *46*, RS1018, doi:10.1029/2010RS004412.
- Gjerloev, J. W. (2009), A Global Ground-Based Magnetometer Initiative, *EOS*, *90*, 27, 230–231.
- Gkioulidou, M., C.-P. Wang, L. R. Lyons, and R. A. Wolf (2009), Formation of the Harang reversal and its dependence on plasma sheet conditions: Rice convection model simulations, *J. Geophys. Res.*, *114*, A07204, doi:10.1029/2008JA013955.
- Gkioulidou, M., C.-P. Wang, and L. R. Lyons (2011), Effect of self-consistent magnetic field on plasma sheet penetration to the inner magnetosphere: Rice convection model simulations combined with modified Dungey force-balanced magnetic field solver, *J. Geophys. Res.*, *116*, A12213, doi:10.1029/2011JA016810.

- Gómez, L., I. S. Juan, A. V. Z. María, M. Amalia, and B. Claudio (2007), Determination of a geomagnetic storm and substorm effects on the ionospheric variability from GPS observations at high latitudes, *J. Atmos. Terr. Phys.*, *69*, 8, 955–968, doi:10.1016/j.jastp.2007.03.002.
- Grebowsky, J. M., H. A. Taylor Jr., and J. M. Lindsay (1983), Location and source of ionospheric high latitude troughs, *Planet. Space Sci.*, *31*, 99–105, doi:10.1016/0032-0633(83)90034-X.
- Harang, L. (1946), The mean field of disturbance of polar geomagnetic storms, *Terr. Magn. Atmos. Electr.*, *51*(3), 353–380, doi:10.1029/TE051i003p00353.
- Heinselman, C. J., and M. J. Nicolls (2008), A Bayesian approach to electric field and E-region neutral wind estimation with the Poker Flat Advanced Modular Incoherent Scatter Radar, *Radio Sci.*, *43*, RS5013, doi:10.1029/2007RS003805.
- Heppner, J. P. (1972), The Harang discontinuity in auroral belt ionospheric currents, *Geophys. Norv.*, *29*, 105–120.
- Inhester, B., J. Untiedt, M. Segatz, and M. Kürschner (1992), Direct determination of the local ionospheric Hall conductance distribution from two-dimensional electric and magnetic field data, *J. Geophys. Res.*, *97*, 4073.
- Jayachandran, P. T., K. Hosokawa, J. W. MacDougall, S. Mushini, R. B. Langley, and K. Shiokawa (2009), GPS total electron content variations associated with a polar cap arc, *J. Geophys. Res.*, *114*, A12304, doi:10.1029/2009JA014916.
- Jones, G. O. L., P. J. S. Williams, K. J. Winser, and M. Lockwood (1990), Characteristics of the high-latitude trough, *Adv. Space Res.*, *10*(6), 1990.
- Karlsson, T., and G. Marklund (1998), Simulations of effects of small-scale auroral current closure in the return current region, *Phys. Space Plasmas*, *15*, 401–406.
- Karlsson, T., N. Brenning, O. Marghitu, G. Marklund, and S. Buchert (2007), High-altitude signatures of ionospheric density depletions caused by field-aligned currents, arXiv:0704.1610v1.
- Kintner, P. M., H. Kil, C. Deehr, and P. Schuck (2002), Simultaneous total electron content and all-sky camera measurements of an auroral arc, *J. Geophys. Res.*, *107*, 1127, doi:10.1029/2001JA000110.
- Kosch, M. J., O. Amm, and M. W. J. Scourfield (2000), A plasma vortex revisited: The importance of including ionospheric conductivity measurements, *J. Geophys. Res.*, *105*(A11), 24,889–24,898, doi:10.1029/2000JA900102.
- Kosch, M. J., M. J. W. Scourfield, and E. Nielsen (1998), A self-consistent explanation for a plasma flow vortex associated with the brightening of an auroral arc, *J. Geophys. Res.*, *103*, 29,383–29,391.
- Lu, G. (2000), A Synthetic view of the magnetospheric-ionospheric current system associated with substorms, in *Magnetospheric Current Systems*, *Geophys. Monogr. Ser.*, vol. 118, edited by S. Ohtani et al., pp. 199–207, AGU, Washington, D. C., doi:10.1029/GM118p0199.
- Ma, S. Y., P. Liu, and K. Schlegel (2000), EISCAT observation of a high-latitude ionization trough associated with a reversed westward plasma flow, *Geophys. Res. Lett.*, *27*(20), 3269–3272, doi:10.1029/2000GL000073.
- Marklund, G. T. (2009), Electric fields and plasma processes in the auroral downward current region, below, within, and above the acceleration region, *Space Sci. Rev.*, *142*, 1–21, doi:10.1007/s11214-008-9373-9.
- McPherron, R. L., C. T. Russell, and M. Aubry (1973), Satellite studies of magnetospheric substorms on August 15, 1978, 9, Phenomenological model for substorms, *J. Geophys. Res.*, *78*, 3131–3149.
- Mende, S. B., et al. (2008), The THEMIS array of ground-based observatories for the study of auroral substorms, *Space Sci. Rev.*, *141*, 357–387, doi:10.1007/s11214-008-9380-x.
- Richards, P. G., D. Bilitza, and D. Voglozin (2010), Ion density calculator (IDC): A new efficient model of ionospheric ion densities, *Radio Sci.*, *45*, RS5007, doi:10.1029/2009RS004332.
- Richmond, A. D., and Y. Kamide (1988), Mapping electrodynamic features of the high-latitude ionosphere from localized observations: Technique, *J. Geophys. Res.*, *93*, 5741–5759, doi:10.1029/JA093iA06p05741.
- Ridley, A. J., and E. A. Kihn (2004), Polar cap index comparisons with AMIE cross polar cap potential, electric field, and polar cap area, *Geophys. Res. Lett.*, *31*, L07801, doi:10.1029/2003GL019113.
- Prikryl, P., P. T. Jayachandran, S. C. Mushini, D. Pokhotelov, J. W. MacDougall, E. Donovan, E. Spanswick, and J.-P. St.-Maurice (2010), GPS TEC, scintillation and cycle slips observed at high latitudes during solar minimum, *Ann. Geophys.*, *28*, 1307–1316, doi:10.5194/angeo-28-1307-2010.
- Prölls, G. W. (2007), The equatorward wall of the subauroral trough in the afternoon/evening sector, *Ann. Geophys.*, *25*, 645–659, doi:10.5194/angeo-25-645-2007.
- Rodger, A. S., R. J. Moffett, and S. Quegan (1992), The role of ion drift in the formation of ionisation troughs in the mid- and high-latitude ionosphere—A review, *J. Atmos. Terr. Phys.*, *54*, 1–30, doi:10.1016/0021-9169(92)90082-V.
- Schunk, R. W., J. J. Sojka, and M. D. Bowline (1987), Theoretical study of the effect of ionospheric return currents on the electron temperature, *J. Geophys. Res.*, *92*, 6013–6022.
- Sellek, R., G. J. Bailey, R. J. Moffett, R. A. Heelis, and P. C. Anderson (1991), Effects of large zonal plasma drifts on the subauroral ionosphere, *J. Atmos. Terr. Phys.*, *53*(6–7), 557–565.
- Williams, P. J. S., and A. R. Jain (1986), Observations of the high latitude trough using EISCAT, *J. Atmos. Terr. Phys.*, *48*(5), 423–434.
- Winser, K. J., G. O. L. Jones, and P. J. S. Williams (1986), A quantitative study of the high latitude ionospheric trough using EISCAT's common programmes, *J. Atmos. Terr. Phys.*, *48*(9–10), 893–904.
- Zettergren, M., J. Semeter, B. Burnett, W. Oliver, C. Heinselman, P.-L. Blelly, and M. Diaz (2010), Dynamic variability in F-region ionospheric composition at auroral arc boundaries, *Ann. Geophys.*, *28*, 651–664, doi:10.5194/angeo-28-651-2010.
- Zhang, B.-C., Y. Kamide, and R.-Y. Liu (2003), Response of electron temperature to field-aligned current carried by thermal electrons: A model, *J. Geophys. Res.*, *108*, 1169, doi:10.1029/2002JA009532.
- Zou, S., L. R. Lyons, C.-P. Wang, A. Boudouridis, J. M. Ruohoniemi, P. C. Anderson, P. L. Dyson, and J. C. Devlin (2009a), On the coupling between the Harang reversal evolution and substorm dynamics: A synthesis of SuperDARN, DMSP, and IMAGE observations, *J. Geophys. Res.*, *114*, A01205, doi:10.1029/2008JA013449.
- Zou, S., L. R. Lyons, M. J. Nicolls, C. J. Heinselman, and S. B. Mende (2009b), Nightside ionospheric electrodynamic features associated with substorms: PFISR and THEMIS ASI observations, *J. Geophys. Res.*, *114*, A12301, doi:10.1029/2009JA014259.
- Zou, S., L. R. Lyons, and Y. Nishimura (2012), Mutual evolution of aurora and ionospheric electrodynamic features near the Harang reversal during substorms, in *Auroral Phenomenology and Magnetospheric Processes: Earth and Other Planets*, *Geophys. Monogr. Ser.*, vol. 197, edited by A. Keiling et al., pp. 159–169, AGU, Washington, D. C., doi:10.1029/2011GM001163.
- Zou, S., M. B. Moldwin, A. Coster, L. R. Lyons, and M. J. Nicolls (2011), GPS TEC observations of dynamics of the mid-latitude trough during substorms, *Geophys. Res. Lett.*, *38*, L14109, doi:10.1029/2011GL048178.